An Effective Method for Milling Tool Condition Monitoring Using On-machine Measurement

Junyi Pang

A Thesis

in

The Department

of

Mechanical, Industrial, and Aerospace Engineering

Presented in Partial Fulfillment of the Requirements

for the Degree of

Master of Applied Science (Mechanical Engineering) at

Concordia University

Montreal, Quebec, Canada

August 2023

CONCORDIA UNIVERSITY

School of Graduate Studies

This is to certify that the thesis prepared

By: **Junyi Pang**

Entitled: **An Effective Method for Milling Tool Condition Monitoring Using On-machine Measurement**

and submitted in partial fulfillment of the requirements for the degree of Master of

Master of Applied Science (Mechanical Engineering)

complies with the regulations of the University and meets the accepted standards with respect to originality and quality.

Signed by the final Examining Committee:

Dr. Youmin Zhang Chair

Dr. Youmin Zhang Examiner

Dr. Hang Xu Examiner

Dr. Zezhong Chen Supervisor

Approved by Dr. Martin Pugh
Chair of Department or Graduate Program Director

Dr. Mourad Debbabi
Dean of Faculty

Date September 12th, 2023

Abstract

An Effective Method for Milling Tool Condition Monitoring Using On-machine Measurement

Junyi Pang

Smart machining technology is now under intensive research worldwide. As a kernel technique of smart machining, on-machine measurement (OMM) technology can automatically measure tool diameter and length with laser tool setters on machine so that the machine controller compensates for the tool wear while machining, which can improve part accuracy without manual tool measurement on tool pre-setters. However, there is a dilemma that the OMM technique cannot predict tool failure so that the operator can replace tools before it fails. To address this problem, this research proposes a new approach to predict failure of round-insert face mill in rough and finish machining to automatically change tools right before their failure. First, the geometric equation of flank wear land width of round-insert face mill is formulated; second, after a tool diameter is measured, the flank wear width is calculated. Third, an experimental method is proposed to determine the tool radius reduction threshold and the tool location of measurement, and then the tool failure can be predicted in rough machining. Then, a new method is established to determine the criteria of tool radius reduction in finish machining according to the machined surface roughness. Finally, several experiments are conducted to verify this approach, and it is applied to a practical example. This approach can be directly applied in industry, and it can advance the smart machining technology.

Keywords: on-machine measurement, tool life prediction, tool condition monitoring, tool wear, surface roughness.

Acknowledgments

I sincerely thank my supervisor, Dr. Zezhong Chen, for his guidance, encouragement, and expertise throughout my research. He not only provided great assistance in my studies but also in my life. I am deeply grateful to him for providing me with the opportunity to conduct experiments in this research. It greatly expanded my practical knowledge and skills in industrial production and enriched my experience.

I would also like to express my gratitude to my colleagues in the lab, Tao Fang, Shaocheng Hu. They generously shared their years of professional knowledge and experience with me and helped me resolve any issues I encountered during the experiments.

Lastly, I would like to thank my family and friends, who have provided me with comfort and support during times of stress. Their support has been instrumental in helping me complete my studies, and they have been the source of motivation that propels me forward.

Table of Contents

List of Figures

List of Tables

Nomenclature

a_p	axial depth of cut
θ_r	flank radial angle
θ_a	flank axial angle
R	insert radius
DR	tool radius wear
β	insert clearance angle
t_i	insert thickness
r	tool radius
L_t	tool length
h	measurement height
R_w	theoretical cutting radius at measurement height
R_f	tool radius with flank wear at measurement height
V_B	flank wear land width

Chapter 1 Introduction

1.1 Background

Computer numerical control (CNC) machining is a dominating method of cutting mechanical part workpieces in industry. Based on the CNC machining technology, intelligent manufacturing is articulated a trend in Industry 4.0 or the Fourth Industrial Revolution. Many advanced technologies are applied to the manufacturing process for higher part accuracy and machining efficiency. CNC machines can be upgraded into smart machines with advanced hardware and software. An important technique in intelligent manufacturing is to integrate workpiece machining and tool measuring with a laser tool setter on machine, which is known as on-machine measurement (OMM).

Traditionally, tool conditions, such as tool radius reduction, length reduction, and flank wear land width, can only be obtained when unloading the tool from the CNC machine and examining it with off-machine equipment, and then the tool wear offset is manually set in the controller for tool path compensation. Since it is inconvenient and time-consuming [1], tool conditions cannot be monitored. Now, OMM is emerging in machining [2]; a laser tool setter is set up and calibrated on the machine table, and then special software in the machine controller automatically measures tool diameter and length with the laser too setter in machining breaks. The tool wear in the controller is updated with the measured tool diameter and length, and then the following tool paths are adjusted to compensate the tool wear in time and to machine parts accurately. There are

different types of tool setters, and the most common tool setters are the touch-probe tool setters and the laser tool setters, as shown in Figure 1.1. The tool setter can automatically measure tool diameter and length during the machining process and can send the actual tool diameter and length to the CNC controller to determine tool wear and to compensate tool wear [3]. The tool measuring process is automatically conducted by the macro programs loaded beforehand, and the measuring job is automated at the pre-planned breaking points of machining. The operator is free from measuring tools.

Comparing the two types of laser tool setters, the laser tool setter is more accurate than the touch-probe tool setter. The laser tool setter has a laser generator and a laser receiver, and a laser beam emits from the generator and the receiver. In measuring, a controller software guides the rotating tool to the laser beam; when it blocks the laser beam by 50%, the spindle location is recorded, and the software calculates the tool diameter or length. Thus, the laser tool setter can measure tool diameter at a height and tool length at a radial offset. For touch-probe tool setters, the touch probe sits on a tripod with electrical current passing through the tripod base circle. When the tool rotating in a reverse way and moving towards the touch probe touches the probe, the electrical current is cut, and a signal is sent to the controller. The controller records the spindle coordinates, and the controller software calculates the tool diameter and length. The laser tool setter is more sensitive than the touch-probe tool setter, thus the laser tool setter is more accurate than that of the touch-probe tool setter [4]. In this research, the laser tool setter is selected in the OMM.

Macros of CNC system software includes some memories of numerical control unit and logic and math operations. A tool measurement program can be developed with macros. This program can guide the tool to the laser beam, block the laser beam, record the tool coordinates, and calculate the tool diameter and length. The main function of the macro program when using the laser tool setter is to store and read different variables in the main program, acquire the current coordinates of the tool, and calculate the tool wear. With the support of the macro programs, the signal sent from the tool setter when triggered by the tool can be processed, and the diameter of the cutting edge can be calculated [5]. The macro program also enables the CNC machine to automatically measure and set the tools without manual intervention, improving efficiency, and reducing setup time.

Figure 1.1 A touch probe tool setter and a laser tool setter are shown.

The OMM technology is an effective method to monitor the condition of the tool. A cutting tool starts to wear the moment it cuts the workpiece. The tool setter is used to measure the radius

of the cutting tool to determine the tool life. Once the tool cutting radius reduction exceeds the threshold, the controller sends warnings immediately so that the cutting tool is replaced to ensure the precision of the machining. Apart from its capability of measuring tool radius and length, a laser tool setter also offers several other functionalities, including tool breakage detection, tool clamping errors, tool identification, run-out measurement, and form deviation.

The on-machine tool setters can only measure the tool radius and cannot measure the width of the flank wear directly. As a result, one of the aims of this thesis is to establish the relationship between the flank wear land width and the tool radius reduction for the milling tool so that the condition of the flank wear can be calculated directly by using the tool setter. Once the geometric relationship between the tool radius and the flank wear land width is determined, the tool wear prediction can be carried out.

1.2 Literature review

1.2.1 Tool wear types in milling

Many kinds of research and experiments have been conducted to study the milling tool wear mechanism. There are seven primary types of wear in milling progress: crater wear, built-up edge, chipping, notch wear, plastic deformation, thermal cracks, and flank wear.

Crater wear is the formation of craters in the rake face of the cutting tool due to a chemical reaction between the workpiece and the tool [6], as shown in Figure 1.2. The crater will extend from the rake face to the cutting edge and decrease the cutting radius of the tool.

Figure 1.2 Crater wear on the rake face of the cutting tool.

A build-up edge usually appears when cutting sticky materials, as shown in Figure 1.3. Workpiece material adheres to the cutting tool instead of being properly cut or removed [7], which increases the cutting radius of the tool. This leads to increased cutting forces, which can result in overall tool failure or the detachment of the built-up edge, often causing the removal of coatings or portions of the cutting edge.

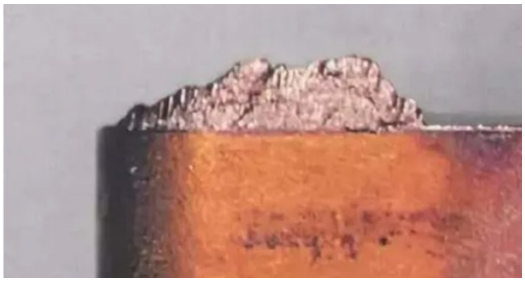

Figure 1.3 Build-up edge adheres to the cutting tool.

Chipping occurs due to an overload of the cutting tool mechanical tensile stress [8], as shown in Figure 1.4. There are several factors that can contribute to these stresses, including chip hammering [9], excessive depth of cut or feed rate [10], built-up edge formation [11], vibrations, or excessive wear on the cutting insert. When these stresses become too high, the cutting edge of the tool can chip, leading to tool failure. Chipping also makes the cutting radius of the tool reduce.

Figure 1.4 Chipping on the cutting edge of the cutting tool.

Notch wear appears at the depth of the cut, as shown in Figure 1.5. It is excessive localized wear that occurs both on the rake and flank face of the tool. Notch wear at the depth of cut occurs because of high-stress gradients [12], fatigue loading [13], and chip adhesion with pull-out [14]. The initial form of notch wear is localized flank wear. As the wear extends both on the rake face and the flank face, it becomes the notch wear. This kind of wear will be detected with an obvious decrease in cutting radius at the depth of cut height using OMM.

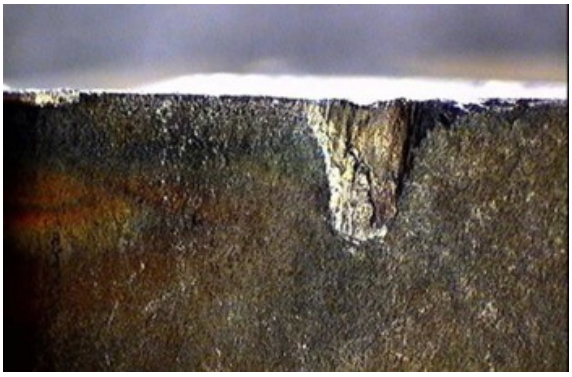

Figure 1.5 Notch wear usually occurs at the depth of the cut.

Plastic deformation occurs when the material of the cutting tool becomes softened due to high cutting temperatures, as shown in Figure 1.6. This phenomenon is more likely to happen with lower-grade cutting tool materials. The deformation results in the tool cutting edge decreasing when being measured using the tool setter.

Figure 1.6 The cutting tool is softened due to temperature.

Thermal cracks are also common during milling. The cracks appear perpendicularly to the cutting edge because of the rapid temperature fluctuations on the cutting edge, mostly due to the cooling condition [15], as shown in Figure 1.7. These cracks also decrease the cutting radius of the

cutting tool and can be detected by the laser tool setter. To avoid thermal cracks, it is recommended to either use a significant amount of coolant or completely abstain from using coolant.

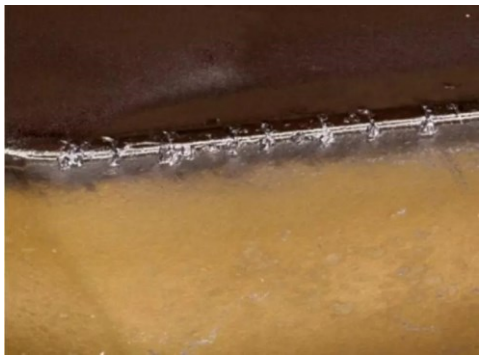

Figure 1.7 Thermal cracks appear due to rapid temperature fluctuations.

Flank wear is the most common type of tool wear that happens on the flank face of the cutting tool, as shown in Figure 1.8. The flank wear occurs due to the continuous contact between the flank face of the tool and the workpiece surface [16], and it will also decrease the measured cutting radius. V_b is the width of the flank wear. If the flank wear extends the tolerance, the surface roughness of the workpiece will be lower than the design requirements, resulting in a decrease in machining accuracy.

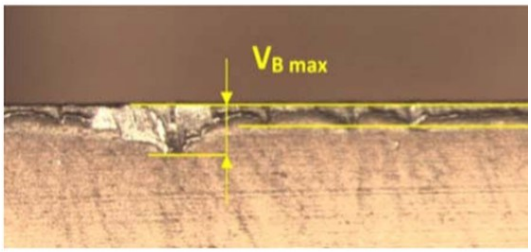

Figure 1.8 Flank wear occurs due to friction.

There are three different types of flank wear in milling, uniform flank wear, non-uniform flank wear and localized flank wear [17]. Uniform flank wear is with constant width and is distributed evenly from zero height to the depth of cut, as shown in Figure 1.9. It is the most expected flank wear as it is predictable. When using the laser tool setter to determine the uniform flank wear, several measurement points can represent the whole tool condition.

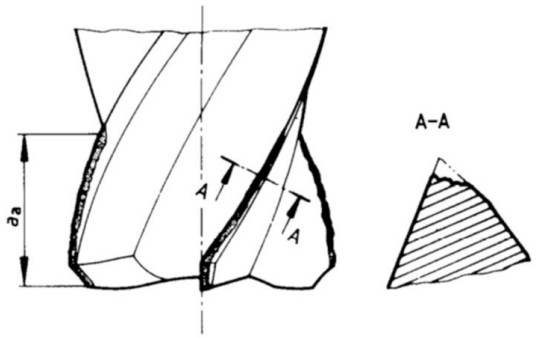

Figure 1.9 The uniform flank wear is the most expected tool wear [25].

The second type of flank wear is non-uniform flank wear (Figure 1.10). The wear pattern is irregular, and when measuring through an on-machine laser tool setter, the cutting radius discretion varies at each measurement height. Usually, when a tool has non-uniform flank wear as its primary wear, the tool condition is determined by the maximum flank wear land width [18].

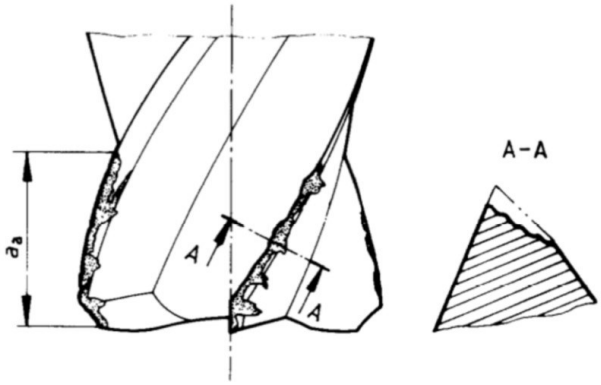

Figure 1.10 The non-uniform flank wear has irregular wear pattern.

The third type of flank wear is localized flank wear, it usually occurs at the locations with maximum stress [19]. The non-uniform flank wear at the depth of cut can develop to notch wear, and its formation may be due to the difference in hardness between the surface material and the internal material of the workpiece [20]. As a result, the locations mentioned above should be set as the primary measurement locations.

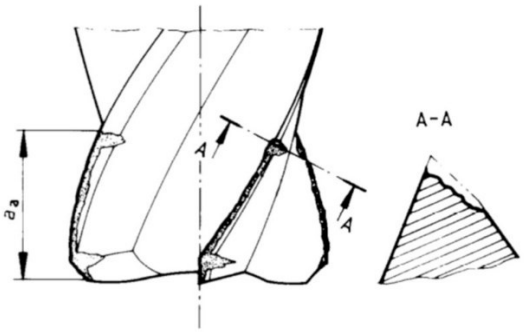

Figure 1.11 The localized flank wear at the locations with maximum stress.

During machining, multiple types of wear may occur before the cutting tool reaches its tool life, and various types of wear may appear under different cutting conditions. Odedeyi *et al.* [21]

performed an experimental study on end milling of stainless steel 316 with coated carbide inserts, and the results showed that the cutting speed is the main factor of the wear type and wear value. When milling at a cutting speed of 146 m/min, the tool wear type was flank wear. When the cutting speed was increased to 205 m/s, both flank wear and build-up edge appeared, and the tool kept milling, then chipping happened on the cutting edge. The results also indicate that in this milling progress, the most heavily worn area appears at the area where the corner radius intersects the side cutting edge. This location is called the junction between the corner rounding and the side cutting edge. Bermingham *et al.* [22] built laser-assisted machining progress. The milling was conducted using a Seco carbide cutting Ti–6Al–4V workpiece. The experiment was at a cutting speed of 90 m/min, a feed rate of 0.28 mm/rev, and a depth of cut of 1 mm. The experiment graphic showed after cutting for 48 seconds, the flank wear was the primary tool wear. The wear was uniform and easy to measure until the cutting time reached 167 s. An obvious notch wear appeared at the depth of the cut, and the tool failed. Emre *et al.* [23] utilized the scanning electron microscope to analyze the tool wear progress while milling NiTi alloy. They proposed that the feed rate is the main factor of the value of the flank wear. The build-up edge was formed near the junction between the corner rounding and the side cutting edge under the condition of low cutting speed and low feed rate since the temperature at the tool-chip interface was low.

It can be noticed that different types of tool wear are always combined to appear before the tool wears out. For most cutting tools, it can be indicated that tool failure always first appears in two locations: one is at the junction between the corner rounding and the side cutting edge of the tool, and the other is at the depth of cut. So, these two locations are considered the optimum measurement locations of most milling tools. As round insert milling tools have different geometric

designs, the optimum measurement locations need to be determined through experiments according to the tool wear patterns.

1.2.2 Tool life determination and prediction

There are several criteria to determine whether a tool reaches its tool life. According to ISO 8688-1 [24], the tool-life criterion can be a pre-determined numerical value representing any measurable form of tool deterioration. If multiple forms of deterioration are measurable, each should be recorded, and once any of the deterioration limits are reached, the tool life has been reached. The deterioration that contributes most to the end of tool life should be used as a guide for selecting the tool life criteria. Two recommended criteria are provided in ISO 8688-2 [25]. One is the depth of the crater on the rake face of the tool, shown in Figure 1.12 (a). In normal conditions, the recommended maximum depth of the crater is 0.1 mm. Another recommended criterion is the width of the flank wear, shown in Figure 1.12 (b). It is the most used criterion, and the uniform maximum value of flank wear land width is recommended as 0.3 mm, while for localized flank wear land width, each tooth of the cutting tool should not be beyond 0.5 mm.

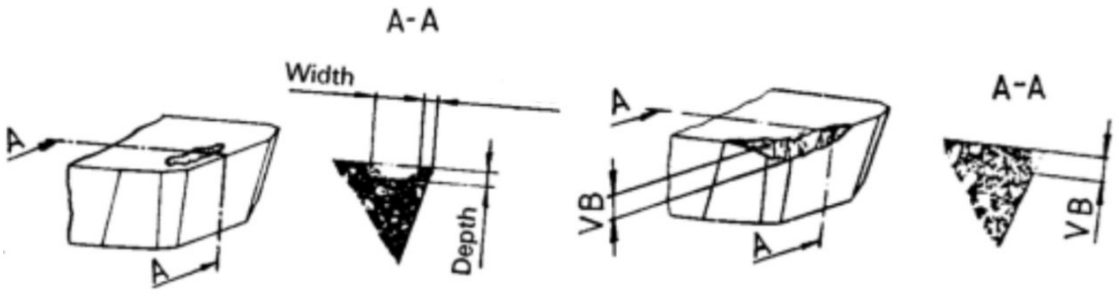

Figure 1.12 (a) The depth of the crater and (b) the flank wear land width [24].

The recommended criteria for tool life determination can only be measured through off-machine measurement and cannot be determined by the on-machine tool setter. The width of the flank wear width is selected most as the primary determinant of the tool life. Once the geometric relationship between the flank wear land width and the tool radius is determined, it is possible to establish a tool life criterion based on the reduction in tool radius.

The tool life curve is shown in Figure 1.13, the wear process of a cutting tool is generally divided into three stages: the Break-in period, the steady state, and the failure period [26]. In the break-in period, the surface of the cutting tool is relatively rough and contains micro-cracks and other defects. The contact area between the tool, workpiece, and chips is small, resulting in high stress on the rake face and flank face of the tool. Consequently, the wear rate of the tool is rapid during this stage. Then after a rapid wear period comes the steady state, which is the effective working period of the tool. As the wear progresses, the flank face gradually becomes smoother. At this stage, the tool enters the normal wear stage, where the wear rate decreases. In the failure region, cutting force and cutting temperature increases, the wear rate also rapidly rises. At this stage, the machine may experience phenomena such as noise and vibration, and the surface quality of the workpiece deteriorates. These indicate that the tool has reached an ineffective wear state. To protect the machine and workpiece, it is necessary to promptly replace the tool.

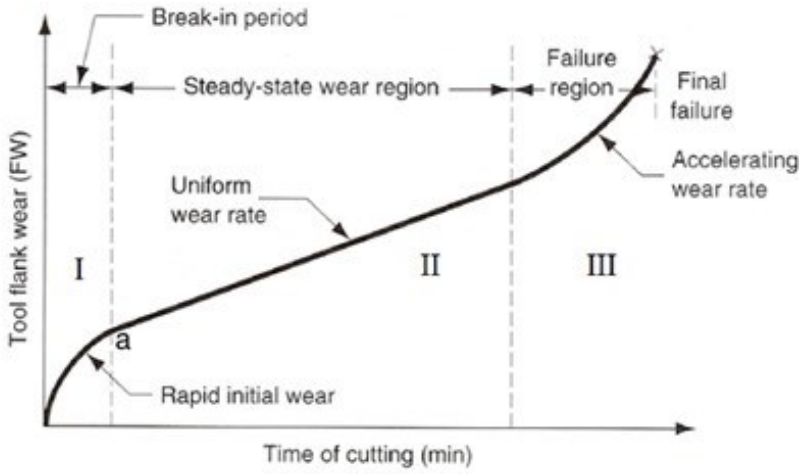

Figure 1.13 Tool life is predicted as a function of cutting time [26].

Tool life prediction has always been an important topic, and researchers have adopted different methodologies to investigate the relationship between tool life and cutting conditions. Alauddin *et al.* [27] utilized response surface contours in speed-feed planes to determine the optimum cutting conditions for the required tool life. The research developed a prediction model for milling steel 190 DHN, and it showed that an increase in the speed, the feed, and the axial depth of cut decrease the tool life. Amir *et al.* [28] performed milling experiments under different conditions by using artificial neural networks and the Taguchi design method. The experiments were out using the high speed steel-E (HSS-E) made cutter and the Al 7075 made workpiece, and the main parameters in the experiments were cutting speed, feed rate and depth of cut, and the test tool life was measured in terms of machining time. The predicted result was close to the experimental data, and the error was 0.006. Jaydeep *et al.* [29] proposed a model to predict flank wear land width using the Bayesian updating method. The carbide inserts and 1018 steel workpieces were used in the experiment. The research investigated the prediction of the flank wear land width with the change of spindle speed under the same other cutting conditions (axial depth

of cut, feed rate), and the result shows that predicted distributions agreed with the experimental values of tool life. Cyril *et al*. [30] predicted the remaining useful life using the neural network technique based on the machine spindle power. The experiment was carried out using carbide inserts cutting stainless steel SS403. The experiment results showed that the accuracy of the prediction model decreases with the decrease in the spindle speed. Yang *et al.* [31] predicted the milling tool life using the model based on trajectory similarity and support vector regression. The relationship between the signal characteristic quantity and the tool wear was studied. The experiment was carried out using a carbide endmill and TC4 workpiece, and the relative errors of flank wear value prediction accuracy in the stable stage of the sample tool were above 88%.

There are many types of research focused on the prediction of flank wear land width. Wang *et al.* [32] proposed a mathematical model of the milling tool's flank wear land width by temperature-dependent wear mechanism determination when machining Inconel 182 overlays. The error of the predicted minimum value and test value is 6.5%. Palanisamy *et al.* [33] plotted contours and response surfaces for the interaction effect of feed rate and depth of cut on tool wear and then applied the artificial neural network to analyze the result and establish a prediction model for flank wear. The model was verified by an experiment cutting AISI 1020 steel with a carbide endmill, and the result showed that the average error between the predicted flank wear and the experiment results is less than 5%. Another tool flank wear prediction model was made by Tiyamike *et al.* [34]. The research developed the VB progression model for face milling of Inconel 718 using multilayer physical vapor deposition TiAlN/NbN coated carbide inserts with the input feature of cutting speed, feed rate, axial depth of cut, and cutting length using a Gaussian kernel ridge regression, the predicted results agreed well with the measure flank wear land width. The experiment results also

showed that different types of tool wear appeared with the increasing cutting time. The uniform flank wear occurred first when the cutting length was 1200 mm, then macro-chipping and localized chipping appeared when the milling length reached 4000 mm. The flank wear and build-up edge were the main type of tool wear on another cutting tool when the milling length was 4400 mm and chipping also appeared at the length of 4600 mm. The tool wear type in the experiment result also meets the theory mentioned in the previous section. Gouarir *et al.* [35] brought up a method to predict the flank wear by training a Convolutional Neural Network, the stainless steel workpiece was milled by a 6 mm Uncoated ball endmill with the substrate of tungsten carbide, the prediction error is less than 10%.

By examining all the prediction models mentioned before, it can be noticed that all the models need significant computational power. However, the CNC controller has limited variables to utilize, and its computational power is limited. So, if the tool condition monitoring and prediction need to be conducted independently on the CNC machine, it is necessary to find an alternative method.

1.2.3 Relationship between flank wear and workpiece surface roughness

In practical industrial manufacturing, the surface roughness of the product is an important criterion, as it directly reflexes the quality of the product. As the tool's flank wears, its cutting edge becomes less efficient, leading to increased friction and heat generation during machining. This can result in poor chip evacuation and surface irregularities, leading to a rougher surface finish. Additionally, excessive flank wear can cause tool vibrations and unstable cutting conditions,

further deteriorating the workpiece surface quality. Therefore, monitoring and controlling flank wear is essential to maintain desired surface roughness in machining operations.

Surface roughness is an important criterion that reflects the tool life in the practical industry. When a tool fails to meet the specified surface roughness requirements, it signifies that the tool has reached the end of its useful life and should be replaced. Uros *et al.* [36] used the adaptive neuro fuzzy inference system (ANFIS) to predict the surface roughness with the different machining variables (spindle speed, feed rate and depth of cut). The ANFIS system was trained, and the resulting prediction error for surface roughness with the experiment result was 4%. Kivak *et al.* [37] built a prediction model using the Taguchi method and regression analysis that predicted both the surface roughness and the flank wear land width with cutting speed and feed rate as machining parameters. The experiment was conducted using Hadfield steel with PVD TiAlN and CVD TiCN/Al2O3-coated carbide inserts under dry milling conditions, and the prediction errors for surface roughness and flank wear land were both within 5%.

There have been several studies on the relationship between surface roughness and tool wear conditions. Kıvak *et al.* [37] milled the Hadfield steel with coated carbide inserts under dry milling conditions. The study found that the feed rate is the main factor for surface roughness, and cutting speed is the main factor for flank wear. The results showed that when the flank wear reached 0.3 mm, the surface roughness of the workpiece was 0.59 μm. Emre *et al.* [23] conducted an experiment to mill the nickel-titanium shape memory alloy with carbide tools. They proposed that the surface roughness is mainly affected by the nose radius of the tool. The results showed that when the flank wear was close to 0.3 mm, the surface roughness of the workpiece was around 0.38

μm, and there was another discovery that the cutting conditions (spindle speed, feed rate and depth of cut) had little effect on the difference of surface roughness as long as the measured flank wear length were the same.

1.3 On-machine measurement system

Before the emergence of on-machine measurement technology, the traditional way to measure the diameter and length of a tool is to use an offline presetter. The offsets of the tool are input into the controller manually by the operators. When the tool condition needs to be checked during the machining, the tool has to be unloaded from the spindle and measured by the offline presetter again. This measurement is very inefficient, and errors due to measurement and installation can easily occur during the progress. With the OMM technology becoming more widely adopted in the industry, tool measurement becomes much more efficient, the measurement does not require unloading the tool and inputting the offsets manually. The controller receives the signal from the tool setter and directly stores the measured radius and length offset values in the corresponding locations, which saves both manpower and time.

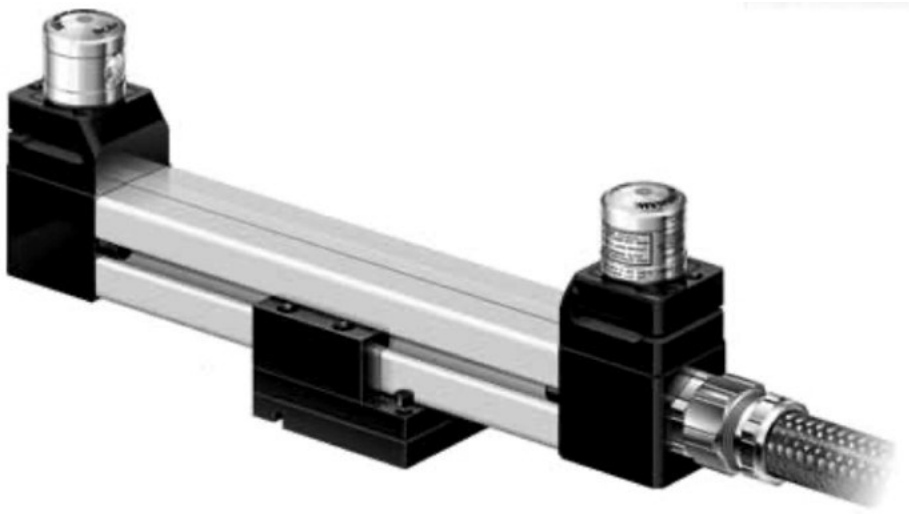

Figure 1.14 The tool setter measures the tools using a laser beam.

The laser tool setter is commonly used in CNC on-machine measurement since it is of high precision and high response speed. The laser tool setter used in this research is a Renishaw NC4 non-contact tool setter, as shown in Figure 1.14. The laser tool setter consists of a laser transmitter and a laser receiver. The receiver has a sensor that detects the laser beam. Once the laser beam is blocked by the tool for fifty percent, the sensor will generate a triggering signal.

The signal triggered by the laser tool setter is sent to an interface (Figure 1.15) that processes the signal from the laser tool setter and converts the signal into a pulse signal that is recognizable by the CNC controller.

Figure 1.15 The interface converts the signal to the controller.

The pulse signal is sent to the CNC controller (Figure 1.16). When the signal is received by the controller, the current coordinates information of the cutting tool is recorded, and the tool geometry condition can be calculated in the CNC controller by calling the macro programs.

Figure 1.16 The CNC controller processes the signal sent from the interface.

The macro programs and the measurement programming software are the core of the whole system. The programs not only enable the CNC machine to measure the tool degradation in radius and length but also provide a method for tool inspection to check for issues such as missing or damaged tool teeth or excessive radial runout of the tool. The laser tool setter, interface, CNC controller, program and software form the intelligent manufacturing system. By applying the system to the industry, the CNC machine can conduct tool geometry measurements and save the information into the controller, then, the new tool path can be generated automatically with the updated tool information, and the tool condition is monitored.

Figure 1.17 shows the designed general workflow of machining progress with OMM. First, the designed model is input to the CAM software to generate the post-processing file, and the G-code is generated for the controller. After loading the file with G-code into the controller, the machining can be started. Before cutting the workpiece, a pre-measurement should be performed to determine the original geometry of the cutting tool and update the tool offsets in the first place. After cutting some parts, the tool needs to be measured, so the macro program is called to perform the on-machine measurement. The controller analyzes the data acquired, calculates the tool wear and determines whether the cutting tool reaches its lifetime. If the tool still functionally works, the newly measured offset value replaces the former value so that the compensated tool path can be generated. If the measured tool wear exceeds the threshold, the machining program will be suspended, and an alert will be sent to replace the tool. The whole process is programmed in advance, and the program can be operated autonomously without intervention.

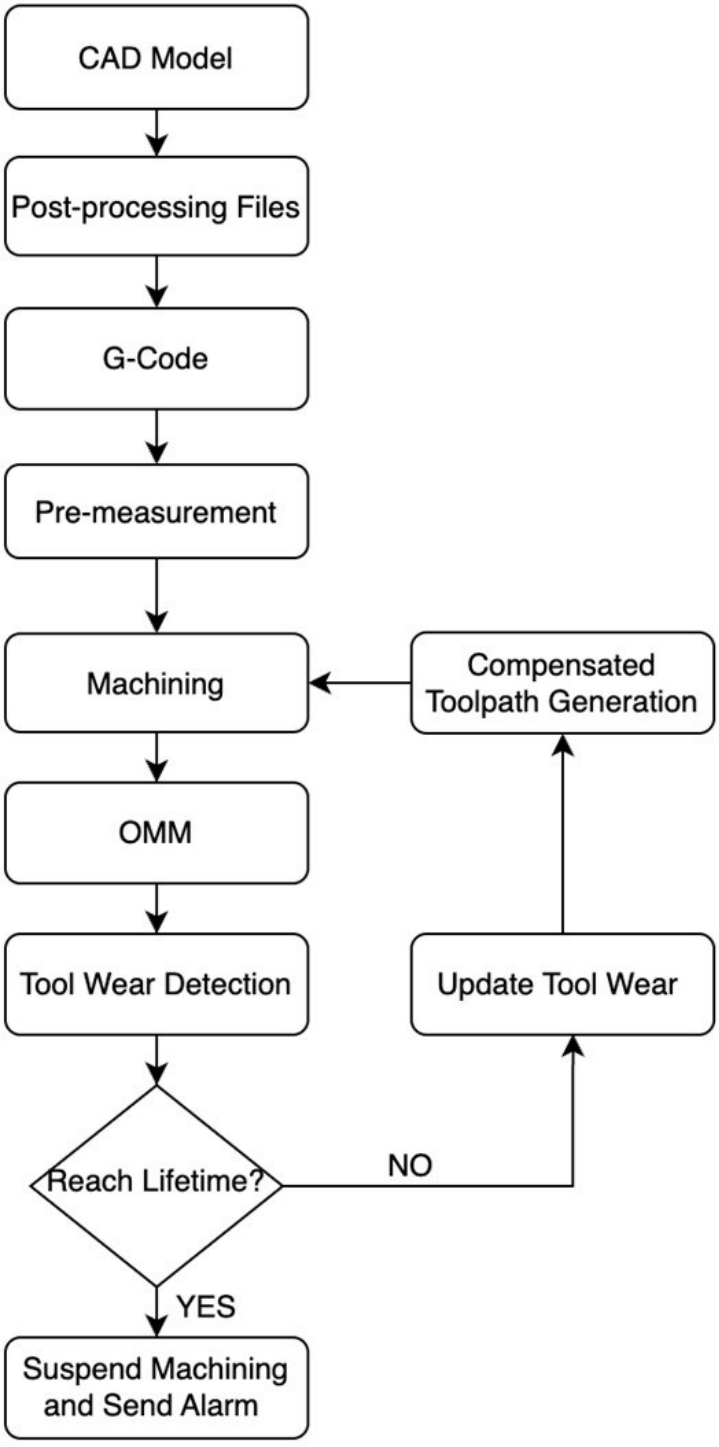

Figure 1.17 The manufacturing progress with OMM technology.

1.4 OMM tool wear threshold for practical industry

The tool life determination mentioned in section 1.2.2 is focused on the tool condition itself. However, if relying only on the method of evaluating tool wear in real industry, there is a risk that the quality of the workpiece may exceed the machining requirements before the tool reaches its wear threshold. In the practical industry, the tool life is usually determined by its cutting time [38], which is also not an accurate method. Some tools are replaced well before reaching their tool life, resulting in unnecessary cost losses. The OMM tool wear threshold in this research is to establish an optimum reference that can determine the tool's life through experimental analysis. The advantage of using the OMM tool wear threshold is that the data can be stored in the CNC controller, enabling the controller to monitor the tool condition independently.

1.5 Thesis objectives and outline

In Chapter 2, a model of a round insert end mill is built, and the tool flank wear mechanism of the insert is demonstrated. In Chapter 3, the geometry relationship between the tool cutting radius decrease and the tool flank wear land width is explained. In Chapter 4, experiments are conducted to verify the accuracy of the flank wear model by applying OMM technique during milling. Then an application of the flank wear theory is conducted to establish the OMM tool wear threshold for roughing and finishing, which demonstrates a method to determine tool life using the flank wear land width and surface roughness. Lastly, Chapter 5 conducts a conclusion.

Chapter 2 Modeling the Flank Wear of a Round Insert End Mill

2.1 Geometric model of a round insert end mill

A model of a round indexable end mill with two inserts is established to simulate the formation progress of the tool insert flank wear, as shown in Figure 2.1.

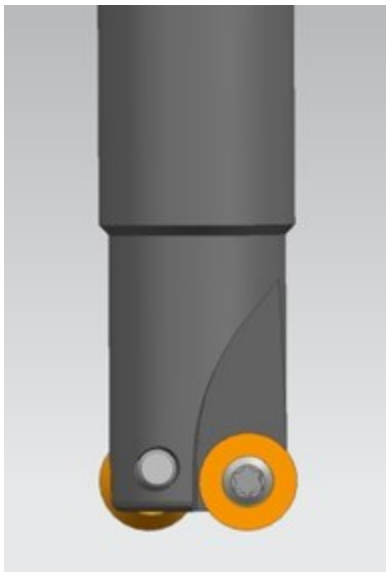

Figure 2.1 A model of an indexable end mill with round inserts is built.

As shown in Figure 2.2 and Figure 2.3, r is the radius of the round insert, and t_i is the thickness of the insert. The virtual cutting point O_1 is the intersection of two tangent lines from point A and point B. The cutting edge is the intersection of the flank face and the rake face from the lowest point of the insert point A to the axial depth of the cut (a_p),

The clearance angle (β) is the angle between the flank face and the workpiece, (see Figure 2.3), which is an important characteristic of the round insert, as the clearance angle directly determines the parametric equation of the flank surface.

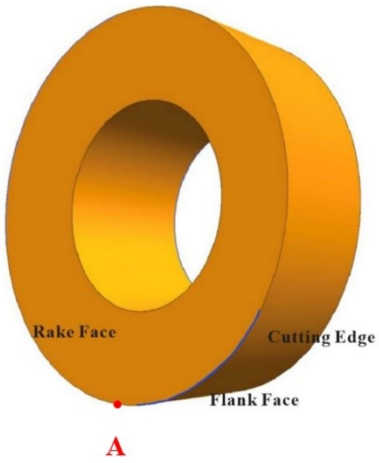

Figure 2.2 A round insert of the cutting tool is shown.

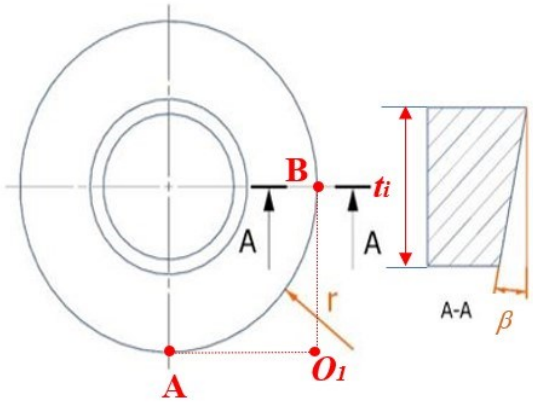

Figure 2.3 The clearance angle and the virtual cutting point of the round insert is shown.

The cutting tool model is with two flutes (see Figure 2.4), and each round insert is fixed into the tool seat with a screw. The cutter seat on the tool body has a radial angle (θ_r) and an axial angle (θ_a) that determine the rake angle of the cutter.

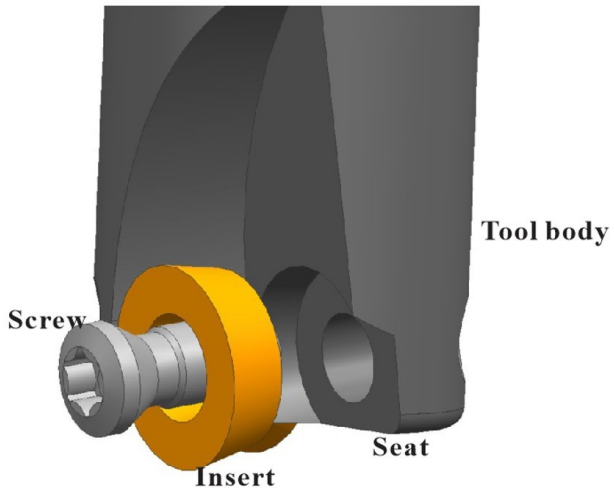

Figure 2.4 The insert is clamped on the tool seat.

To better determine the rake angle, a zero-height plane is introduced, which is a horizontal plane at the lowest point of the cutting tool. O_t is the intersection of the tool body axis and the zero-height plane, and the distance between O_t and the virtual cutting point O_i is determined as the tool's radius. The extension of the rake face intersects the zero-height plane at line O_iP. The radial angle (θ_r) of the insert is the angle between O_t O_i and O_iP, as shown in Figure 2.5. The axial angle of the round insert (θ_a) is the complementary angle of the angle between the rake face and the zero-height plane (see Figure 2.6). When an insert is screwed into the cutting tool seat, the position is settled, but during the milling process, tool wear will occur and will change the geometry of the insert. As

a result, the tool wear mechanism is studied to adjust and update the insert's geometry to minimize manufacturing errors.

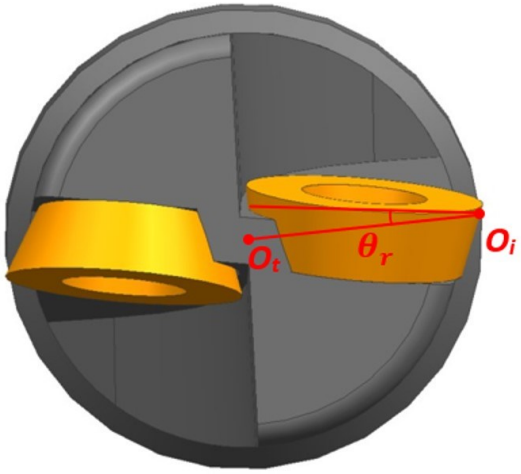

Figure 2.5 The radial angle of the round insert.

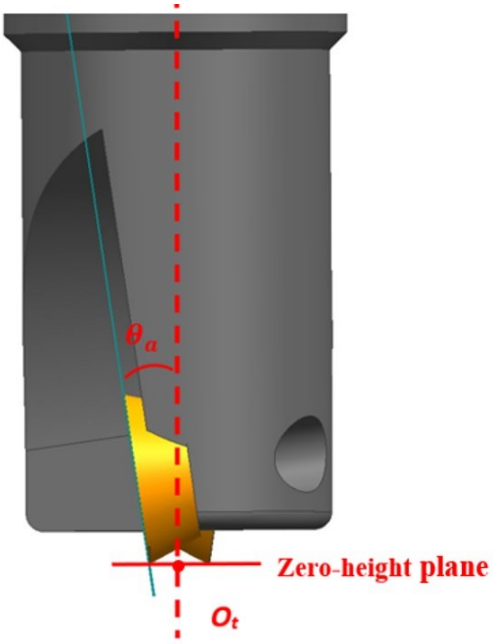

Figure 2.6 The axial angle of the round insert.

2.2 Geometric analysis of the flank wear mechanism

The flank wear mechanism is analyzed in this section. Because of the friction between the tool flank face and the workpiece surface, the flank wear will appear, and the flank wear land width will grow until the insert fails. As the width of the flank wear increases, the radius of the cutting edge decreases, so there is a relationship between the value of the flank wear width and the tool cutting edge radius decrease. To numerically analyze this relationship, the round indexable flank wear progress simulation is built in the first place.

For an intact insert without wear, the cutting edge of the indexable round mill rotates around the spindle axis, and the rotation of the cutting edge forms the rotation surface (see Figure 2.7). When the milling progress starts, the insert starts to wear, and abrasion starts to appear on the flank surface and the cutting edge. Therefore, a new cutting edge is formed.

Figure 2.7 The original rotation surface of the round insert is formed.

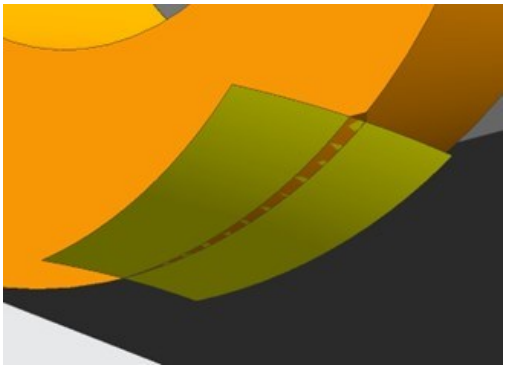

Figure 2.8 The new rotation surface of the round insert with flank wear is formed.

The new cutting edge forms a new rotation surface. The new rotation surface is shown in Figure 2.8. This tool wear model is made based on the assumption that the primary type of tool wear of the round insert indexable mill is flank wear. The reason for this assumption is that flank wear is usually the most common type of wear. Flank wear appears when the milling starts and is always used for examining the tool life of the insert.

The model is built by reducing the radius of the original cutting edge rotation surface in the direction of the spindle axis to simulate the progress of the formation of the new cutting edge rotation surface, the area between the two intersections of the new rotation surface and the insert is the flank wear land.

With this flank wear land model established, the flank wear mechanism can be numerically analyzed in the next chapter. As seen during the progress of building the model, the flank wear directly affects the cutting edge radius, so the tool setter can get the width of the flank wear by measuring the radius of the tool. The specific method to calculate the flank wear land of the round insert using the tool radius reduction is explained in the following chapter.

Chapter 3 Relationship Between Cutting Edge Radius Reduction and Flank Wear Land Width

3.1 Parametric equations of the flank surface on the round insert

To numerically analyze the relationship between the flank wear land width and the radius of the round insert, the first step is to establish the parametric equations of the flank surface. The round insert flank surface is a frustum of a right circular cone. Assuming the rake angle of the surface is zero, the parametric equations of the insert are derivate. First, the insert coordinate system (X_i- Y_i - Z_i - O_i) is set in the center of the insert, and the surface X_i - Z_i - O_i is on the rake surface of the insert, as shown in Figure 3.1.

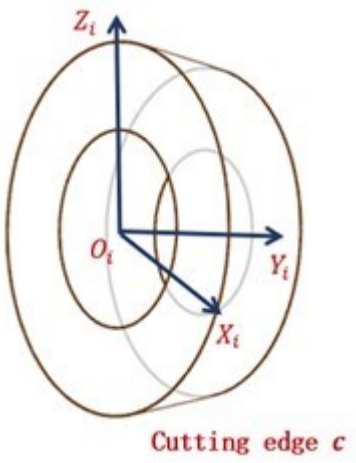

Figure 3.1 The insert coordinate system and the cutting edge is shown

After the coordinate system is built, the parametric equation of the round insert in this coordinate system can be derived as

$$E_{\mathrm{i}} = \begin{bmatrix} x_i \\ y_i \\ z_i \\ 1 \end{bmatrix} = \begin{bmatrix} (R - t \cdot \tan(\beta)) \cdot \cos(\alpha) \\ \mathrm{t} \\ (R - t \cdot \tan(\beta)) \cdot \sin(\alpha) \\ 1 \end{bmatrix}, \quad 0 \le \alpha \le 2\pi \text{ and } 0 \le t < t_{\mathrm{i}} \tag{3.1}$$

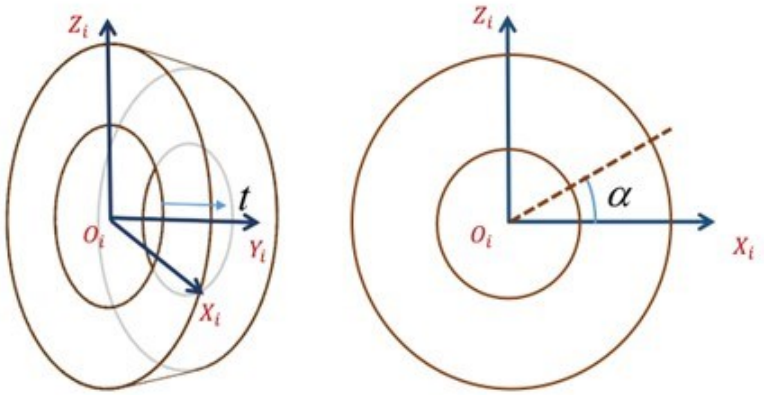

Figure 3.2 Parameterization of the round insert.

Where R is the radius of the round insert, t is the thickness parameter of the insert, and α is the angle parameter with respect to O_iY_i axis. t_i is the thickness of the insert and β is the clearance angle of the insert. The cutting edge of the insert is a circle, as shown in Figure 3.1. Its parametric equation is

$$c_i = \begin{bmatrix} R \cdot \cos(\lambda) \\ 0 \\ R \cdot \sin(\lambda) \\ 1 \end{bmatrix} \qquad -\frac{\pi}{2} \le \lambda \le 0 \tag{3.2}$$

3.2 Transformation matrix from the insert to the tool coordinate system

After the parametric equations of the round insert are established in the insert coordinate system (X_i- Y_i - Z_i - O_i), the next step is to derivate the parametric equations of the insert in the tool coordinate system. The tool coordinate system (X_t- Y_t - Z_t - O_t), is shown in Figure 3.3. Point L is the lowest point of the cutting edge, and the X_t O_t Y_t surface is set on this height.

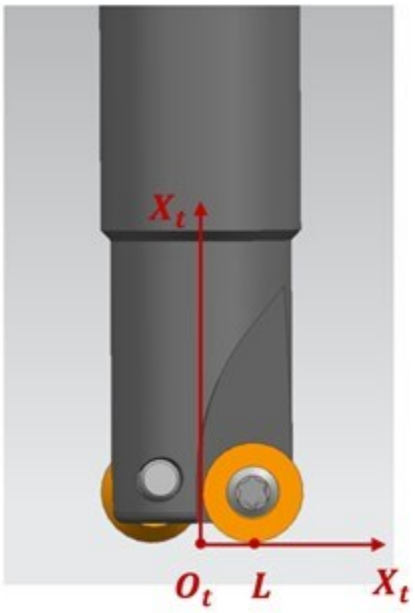

Figure 3.3 The tool coordinate system is established.

The O_tZ_t axis is along the spindle axis and the O_tX_t axis is along the line O_tO_1, where O_1 is the virtual cutting point of the round insert. According to the definition of the virtual cutting point, O_tO_1 is the maximum cutting radius of the tool (r). The O_tY_t axis is set following the right-hand rule.

The way to derivate the parametric equations of the round insert in the tool coordinate system is to use the transformation matrix. The geometric relationship between the two coordinate systems is shown in Figure 3.4. When the insert is clamped into the cutter, the virtual cutting point O_1 is on the $X_tO_tY_t$ surface. The axial angle (θ_a) of the insert is defined as the angle between O_iZ_i axis and O_tZ_t axis, and the radial angle (θ_r) is defined as the angle between O_iX_i axis and O_tX_t axis.

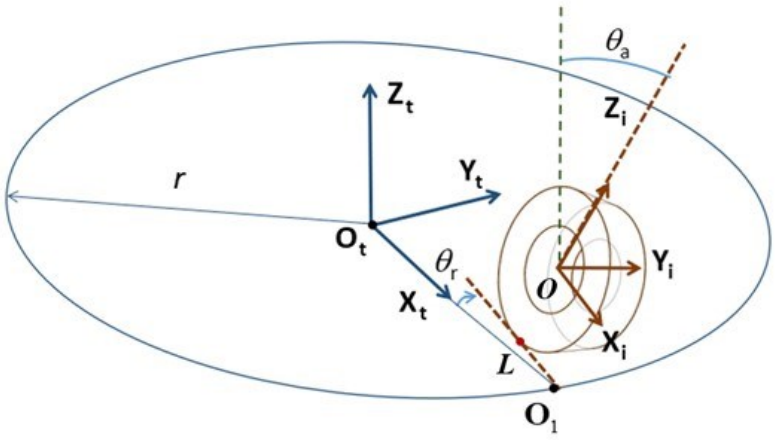

Figure 3.4 The insert can be located in the tool coordinate system.

The virtual cutting point O_1 is an important point during the transformation progress. The coordinate system needs to be translated to O_1 from the insert coordinate system first, shown in

Figure 3.5. The rake surface of the insert is coplanar with the $O_1 X_1 Z_1$, and the origin of this coordinate is at O_1, $O_1 X_1$ axis is colinear with the line $O_1 L$, and now X_1- Y_1 - Z_1 - O_1 is the coordinate system at the virtual cutting point.

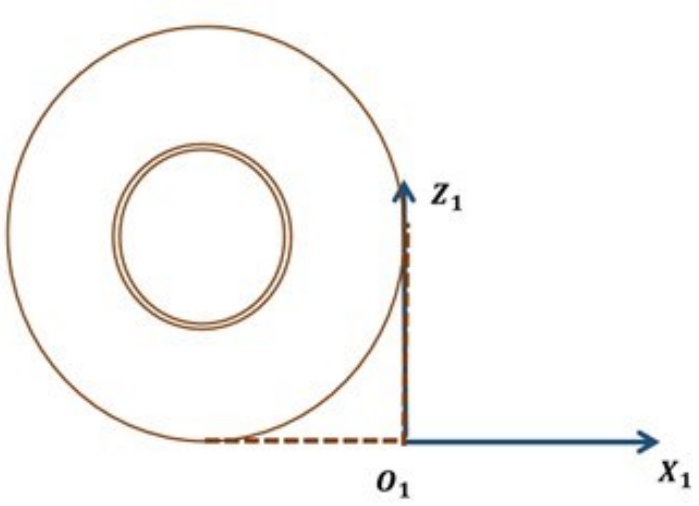

Figure 3.5 The coordinate system at the virtual cutting point is established.

The translation matrix for moving the insert coordinate system to the virtual cutting point is to move the coordinate system r in the X_i direction and then move -R in the Z_i direction. The translation matrix is

$$T_i = \begin{bmatrix} 1 & 0 & 0 & -R \\ 0 & 0 & 0 & 0 \\ 0 & 0 & 0 & R \\ 0 & 0 & 0 & 1 \end{bmatrix} \qquad (3.3)$$

To transfer the coordinate system X_1- Y_1 - Z_1 - O_1 to the same direction as the tool coordinate system X_t- Y_t - Z_t - O_t, it should be first rotated about the X_1 axis by θ_a, the rotation matrix is

$$R_{X1} = \begin{bmatrix} 1 & 0 & 0 & 0 \\ 0 & \cos(\theta_a) & \sin(\theta_a) & 0 \\ 0 & -\sin(\theta_a) & \cos(\theta_a) & 0 \\ 0 & 0 & 0 & 1 \end{bmatrix}. \quad (3.4)$$

Then the coordinate system should be rotated about the Z_1 axis by θ_r, the rotation matrix is

$$R_{Z1} = \begin{bmatrix} \cos(\theta_r) & \sin(\theta_r) & 0 & 0 \\ -\sin(\theta_r) & \cos(\theta_r) & 0 & 0 \\ 0 & 0 & 1 & 0 \\ 0 & 0 & 0 & 1 \end{bmatrix} \quad (3.5)$$

The final step is to translate the coordinate system at the virtual cutting point to the tool coordinate system. The coordinate system should be moved in the X_t direction by r, and the translation matrix is

$$T_r = \begin{bmatrix} 1 & 0 & 0 & r \\ 0 & 1 & 0 & 0 \\ 0 & 0 & 1 & 0 \\ 0 & 0 & 0 & 1 \end{bmatrix} \quad (3.6)$$

So the equivalent transformation matrix from the insert coordinate system to the tool coordinate system is

$$
{}^{T}_{\mathrm{i}}M = T_r \cdot R_{Z1} \cdot R_{X1} \cdot T_i =
$$

$$
\begin{bmatrix} 1 & 0 & 0 & r \\ 0 & 1 & 0 & 0 \\ 0 & 0 & 1 & 0 \\ 0 & 0 & 0 & 1 \end{bmatrix} \cdot \begin{bmatrix} \cos(\theta_r) & \sin(\theta_r) & 0 & 0 \\ -\sin(\theta_r) & \cos(\theta_r) & 0 & 0 \\ 0 & 0 & 1 & 0 \\ 0 & 0 & 0 & 1 \end{bmatrix} \cdot \begin{bmatrix} 1 & 0 & 0 & 0 \\ 0 & \cos(\theta_a) & \sin(\theta_a) & 0 \\ 0 & -\sin(\theta_a) & \cos(\theta_a) & 0 \\ 0 & 0 & 0 & 1 \end{bmatrix} \cdot \begin{bmatrix} 1 & 0 & 0 & -R \\ 0 & 0 & 0 & 0 \\ 0 & 0 & 0 & R \\ 0 & 0 & 0 & 1 \end{bmatrix} \tag{3.7}
$$

$$
= \begin{bmatrix} \cos(\theta_r) & \cos(\theta_a) \cdot \sin(\theta_r) & \sin(\theta_a) \cdot \sin(\theta_r) & r - \cos(\theta_r) \cdot R + R \cdot \sin(\theta_a) \cdot \sin(\theta_r) \\ -\sin(\theta_r) & \cos(\theta_a) \cdot \cos(\theta_r) & \cos(\theta_r) \cdot \sin(\theta_a) & R \cdot \sin(\theta_r) + \cos(\theta_r) \cdot R \cdot \sin(\theta_a) \\ 0 & -\sin(\theta_a) & \cos(\theta_a) & \cos(\theta_a) \cdot R \\ 0 & 0 & 0 & 1 \end{bmatrix}
$$

3.3 Calculation of the flank wear land width on the round insert indexable mill

The laser tool setter only measures the change of the cutting radius, so if the flank wear land is to be calculated by the on-machine laser tool setter indirectly, the first step is to derivate the parametric equations of the flank surface from the insert coordinate system to the cutting tool system. The parametric equation of the flank surface in the tool coordinate system is

$$E_t = {}^{T}_{\mathrm{i}}M \cdot E_i = \begin{bmatrix} x_t \\ y_t \\ z_t \\ 1 \end{bmatrix}$$

$$= \begin{bmatrix} \cos(\theta_r)J\cos(\alpha) + t\cos(\theta_a)\sin(\theta_r) + J)\sin(\alpha)\sin(\theta_a)\sin(\theta_r) + r + R(\sin(\theta_a)\sin(\theta_r) - \cos(\theta_r)) \\ \mathrm{t}\cos(\theta_a)\cos(\theta_r) - \sin(\theta_r)\cos(\alpha)J + \cos(\theta_r)\sin(\theta_a)J\sin(\alpha) + R(\sin(\theta_r) + \sin(\theta_a)\cos(\theta_r)) \\ -\sin(\theta_a)t + \cos(\theta_a)J\sin(\alpha) + R\cos(\theta_a) \\ 1 \end{bmatrix} \tag{3.8}$$

Where $J = R - t\tan\beta$.

When measuring the tool radius using the laser tool setter, a measurement height (h) needs to be set, as shown in Figure 3.6. The laser tool setter detects the cutting edge at point P_w, and the controller of the CNC machine calculates the tool radius at this measurement height, then sends the new tool radius back to the offset for tool radius compensation.

Given a measurement height, the theoretical tool radius (R_w) of a cutting edge with unworn inserts can be calculated. The cutting edge c intersects the surface of the measurement height at point P_w. The theoretical cutting radius is calculated using the parametric equation of the cutting edge of the insert, as mentioned in equation 3.2. By transferring the parametric equation of the cutting edge from the insert coordinate system to the tool coordinate system using the transformation matrix, the parametric equation of the cutting edge in the tool coordinate system is

$$c_t(\lambda) = {}^{T}_{\mathrm{i}}M \cdot c_i(\lambda) \tag{3.9}$$

When a measurement height h is determined, h equals to Z_W, the cutting edge intersects with the horizontal surface at measurement height h. The geometric relationship between h and the angle parameter of the cutting edge λ can be established as

$$\sin(\lambda) = \frac{h}{\cos(\theta_a)R} - 1 \tag{3.10}$$

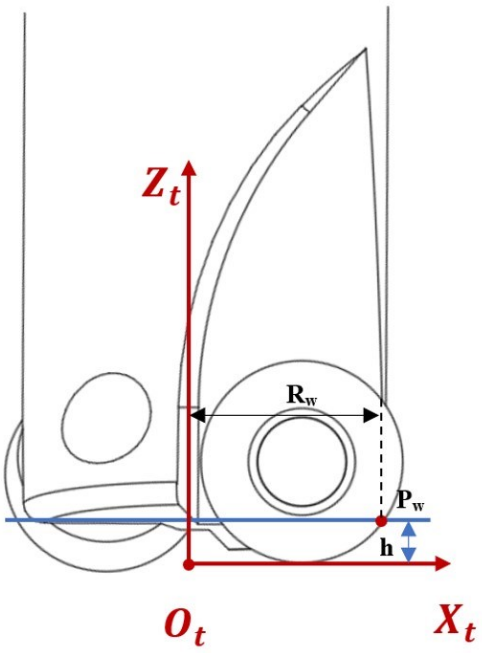

Figure 3.6 Measuring the tool cutting radius at the measurement height.

P_w is a point on the cutting edge at the measurement height. Its coordinates are calculated by replacing λ with h R and $\cos(\theta_a)$ in equation 3.9.

$$P_w = \begin{bmatrix} x_w \\ y_w \\ z_w \\ 1 \end{bmatrix} = \begin{bmatrix} r - \cos(\theta_r)R + \cos(\theta_r)RG + \tan(\theta_a)\sin(\theta_r)h \\ R\sin(\theta_r) - R\sin(\theta_r)G + \cos(\theta_r)\tan(\theta_a)h \\ h \\ 1 \end{bmatrix} \tag{3.11}$$

where $G = (1 - (\frac{\cos(\theta_r)h - R}{R})^2)^{\frac{1}{2}}$.

So the tool cutting radius at the measurement height (R_w) can be calculated using the coordinates of point P_w

$$x_w{}^2 + y_w{}^2 = R_w{}^2 \tag{3.12}$$

The tool radius wear is DR, so the newly formed cutting radius of the tool (R_f) can be calculated, and point P_f shown in Figure 3.7 is the intersection of the new tool cutting edge with the horizontal surface at measurement height.

$$R_f = R_w - DR \tag{3.13}$$

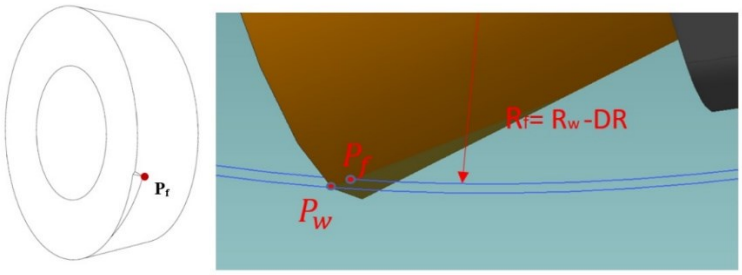

Figure 3. 7 The newly formed tool cutting radius Rf.

To calculate the flank wear land, the coordinates of point P_f needs to be obtained. As point P_f is on both the circle with a radius of R_f and the flank surface, the coordinates of the P_f (x_f, y_f, z_f) can be obtained by solving the equations:

$$\begin{cases} {x_f}^2 + {y_f}^2 = {R_f}^2 \\ z_f = \mathrm{z}_t = h \end{cases} \tag{3.14}$$

First, the parameter t can be calculated by using $z_w = \mathrm{z}_t = h$:

$$t = \frac{R(\sin\alpha + 1) - h}{\tan(\theta_a) + \tan\beta \sin\alpha} \tag{3.15}$$

Then the parameter t in Equation 3.8 can be replaced by α, and the equations are only functions of α :

$$P_f = \begin{bmatrix} x_f \\ y_f \\ z_f \\ 1 \end{bmatrix}' = \begin{bmatrix} A + B\cos\alpha + C\sin\alpha \\ D + E\cos\alpha + F\sin\alpha \\ h \\ 1 \end{bmatrix}' \tag{3.16}$$

Where

$$A = R\cos\theta_r - \frac{T - \cos\theta_r}{Q} + V$$

$$B = -\frac{-\cos\theta_r P\tan\beta}{Q}$$

$$C = \frac{S\cos\theta_r}{Q} + U$$

$$D = \frac{P}{Q}\cos\theta_a\cos\theta_r + R(\sin\theta_r + \sin\theta_a + \cos\theta_r)$$

$$E = -R\sin\theta_r + \frac{P}{Q}\sin\theta_r\tan\beta$$

$$F = \cos\theta_r\sin\theta_a(R - \frac{P}{Q}\tan\beta)$$

$$P = R(\sin\alpha + 1) - h$$

$$Q = \tan\theta_a + \tan\beta\sin\alpha$$

$$S = \tan\beta\sin\theta_r\sin\theta_a$$

$$T = \cos\theta_a\sin\theta_r$$

$$U = R\sin\theta_r\sin\theta_a$$

$$V = r + R(\sin\theta_r\sin\theta_a - \cos\theta_r)$$

The flank wear land width is defined as the vertical distance from point P_f to the rake face of the insert. To calculate this value, the equation of the rake face in the tool coordinate system needs to be derived.

The unit normal vector of the rake face in the insert coordinate ${}^{i}\boldsymbol{i}_{r}$ system is

$$ {}^{i}i_{r} = \begin{bmatrix} 0 \\ 1 \\ 0 \\ 1 \end{bmatrix}. \tag{3.17} $$

By using the transformation matrix, the normal vector of the rake face in the tool coordinate system ${}^{t}\boldsymbol{i}_{r}$ is

$$ {}^{t}i_{r} = R_{Z1} \cdot R_{X1} \cdot {}^{i}i_{r} = \begin{bmatrix} A_t \\ B_t \\ C_t \\ 1 \end{bmatrix} = \begin{bmatrix} \cos\theta_a \sin\theta_r \\ \cos\theta_a \cos\theta_r \\ -\sin\theta_a \\ 1 \end{bmatrix}. \tag{3.18} $$

Then the equation of the rake face in the tool coordinate system can be presented as:

$$ A_t \cdot (x - r) + B_t \cdot y + C_t \cdot Z = 0 \tag{3.19} $$

The flank wear land width (V_B) can be calculated using the distance formula:

$$ V_B = \frac{\left| A_t \cdot (X_f - r) + B_t \cdot X_f + C_t \cdot h \right|}{\sqrt{A_t^2 + B_t^2 + C_t^2}} \tag{3.20} $$

With Equation 3.20 being established, the flank wear land width at measurement height *h* can be calculated.

Chapter 4 Experimental Verification of Flank Wear Mechanism of a Round Insert Mill

4.1 Experimental design

To verify the relationship between the flank wear and the cutting radius reduction of the round insert, and to study the tool wear pattern of the tool, a verification experiment should be conducted. The OMM system is introduced into the experiment to measure the cutting radius of the tool, and the images of the tool wear are taken with the microscope.

The experiment procedure is as follows: The milling program is input to the CNC controller for machining. The laser tool setter is utilized by calling the tool setter's macro program within the main program. Every time the tool is measured by the laser tool setter, the value of the radius offset stored by the controller should be recorded. The cutting tool is unloaded from the spindle to measure the flank wear land width on the microscope. When measuring the flank wear land width of the insert, the microscope measurement should be in the direction parallel to the rake face of the insert and perpendicular to the cutting edge.

The cutting tool machines a block-shaped workpiece. During the process of milling the workpiece, the insert cuts the workpiece and wears out. A cut is defined as the tool machining one layer of the workpiece with a depth of 1mm (see Figure 4.1). The measurement is taken after every

cut, and the predicted flank wear land width is compared with the experimental result to verify the accuracy of the flank wear land width model.

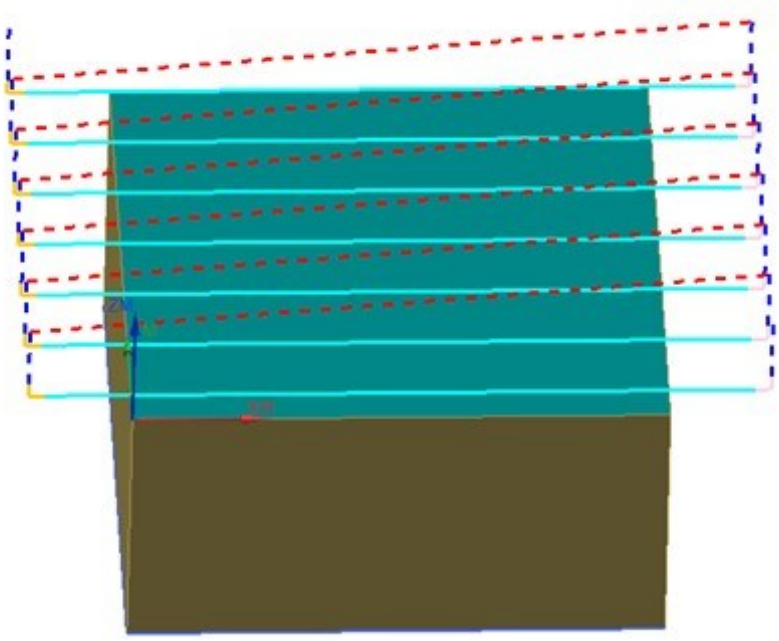

Figure 4.1 One cut is defined as the cutting tool milling one layer of the workpiece.

4.2 Experimental setup

The experiments are conducted on the Bridgeport VMC 1000xp 3-axis CNC machine, which is equipped with a FANUC Oi Mate-MD controller, as shown in Figure 4.2. The EMR5R two inserts round mill is selected, as shown in Figure 4.3, the insert material is H5501 alloy with coating. The tool radius and the tool length are measured by a tool presetter before being loaded on the spindle, and the tool parameters are listed in Table 4.1. A Renishaw NC4 laser tool setter is installed on the CNC machine to construct the OMM system, as shown in Figure 4.4. This is a roughing machining process, the 104 by 104 by 40 mm 2Cr13 stainless steel workpiece is clamped

on the worktable (Figure 4.5), and the tool cuts the workpiece without coolant. After the cut, the tool is unloaded from the spindle and observed under the microscope (see Figure 4.6). The axial depth of cut is set as 1 mm, the radial depth of cut is 5 mm the spindle speed is 2000 rev/min, and the feed rate is 700 mm/min. The measurement points are evenly distributed from zero to the depth of cut in the tool axis direction, and the height of each measurement from P_1 to P_5 is as follows: 0.2 mm, 0.4 mm, 0.6 mm, 0.8 mm, and 1 mm, as shown in Figure 4.7.

Figure 4.2 The Bridgeport VMC 1000xp 3-axis CNC machine is selected for milling.

Figure 4.3 The EMR5R two inserts round mill is selected for milling.

Table 4.1 The parameters of the EMR5R cutting tool.

Parameters	Symbols	Values
Tool radius	r	5.024 mm
Tool length	L_t	176.792 mm
Insert axial angle	θ_a	6°
Insert radial angle	θ_r	-12°
Clearance angle	β	10°
Insert radius	R	5 mm
Insert thickness	t_i	3 mm

Figure 4.4 The round inset tool is measured by the OMM system.

Figure 4.5 The 2Cr13 stainless steel workpiece is fixed for milling.

Figure 4.6 The tool wear is observed under the microscope.

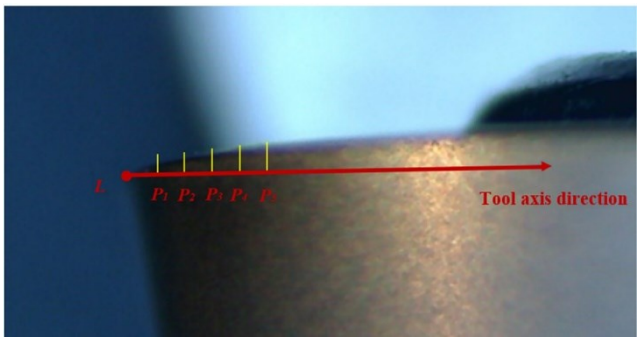

Figure 4.7 The measurement points are distributed evenly along the tool axis direction.

4.3 Results and discussion

Before the cut, the cutting radii at five measurement heights are measured by the laser tool setter to determine the initial tool cutting radii, each point is measured three times and the average value is measured as the result. As the tool length is not decreasing during each measurement, the tool length wear is negligible. The results are shown in Table 4.2. The cutting tool is measured by the laser tool setter after machining each layer of the workpiece, the tool radii at 5 measurement points are recorded by the controller and stored in the controller system variables, then the tool is unloaded from the spindle to measure the flank wear land width by the microscope. The tool wear patterns of the two inserts A and B are shown below (Figure 4.8 to Figure 4.14), and the measured and predicted insert flank wear land width are compared in the table (Table 4.3 to Table 4.8). Since the differences in tool flank wear land width between inserts A and B are both less than 0.01 mm, the values of the tool flank wear land widths presented in the tables represent the average measurements taken from both inserts at each measurement point.

Table 4.2 The initial cutting radii of the tool.

Measurement point	1	2	3	4	5
Tool radius (mm)	6.671	7.197	7.591	7.910	8.180

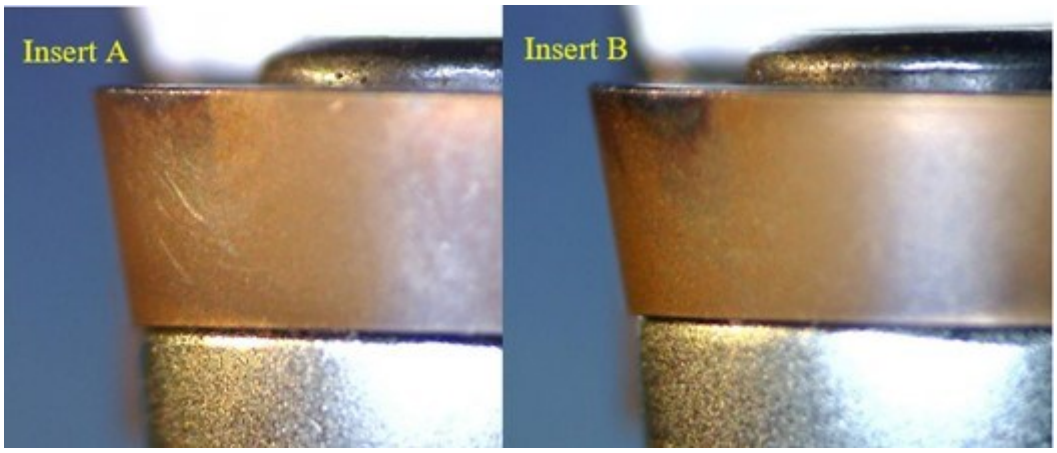

Figure 4.8 The wear images of insert A and B after milling one layer of the workpiece.

Table 4.3 The cutting radii and flank wear after milling one layer of the workpiece.

Measurement point	1	2	3	4	5
Tool radius (mm)	6.663	7.170	7.564	7.874	8.148
Radius wear (mm)	0.008	0.027	0.027	0.030	0.03
Measured V_B (mm)	0.012	0.051	0.055	0.0780	0.080
Predicted V_B (mm)	0.013	0.049	0.059	0.0745	0.083
Error	7.69%	4.08%	6.78%	4.70%	3.61%

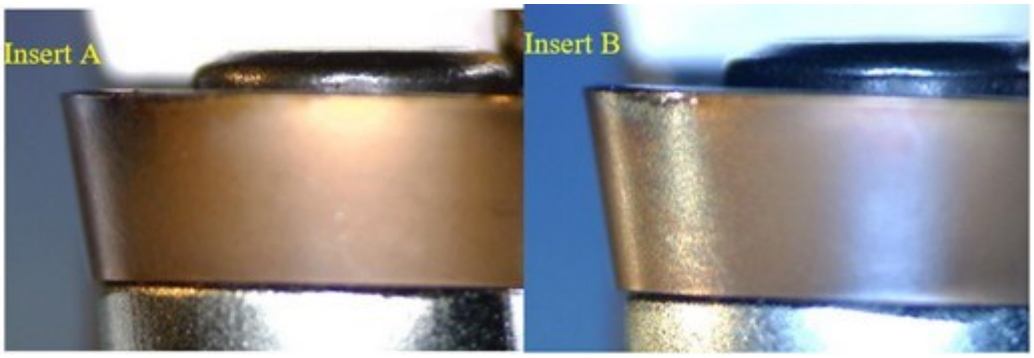

Figure 4.9 The wear images of insert A and B after milling two layers of the workpiece.

Table 4. 4 The cutting radii and flank wear after milling two layers of the workpiece.

Measurement point	1	2	3	4	5
Tool radius (mm)	6.650	7.169	7.556	7.878	8.154
Radius wear (mm)	0.021	0.028	0.035	0.032	0.031
Measured V_B (mm)	0.031	0.054	0.075	0.075	0.081
Predicted V_B (mm)	0.029	0.050	0.074	0.079	0.085
Error	6.90%	8.00%	1.35%	5.06%	7.06%

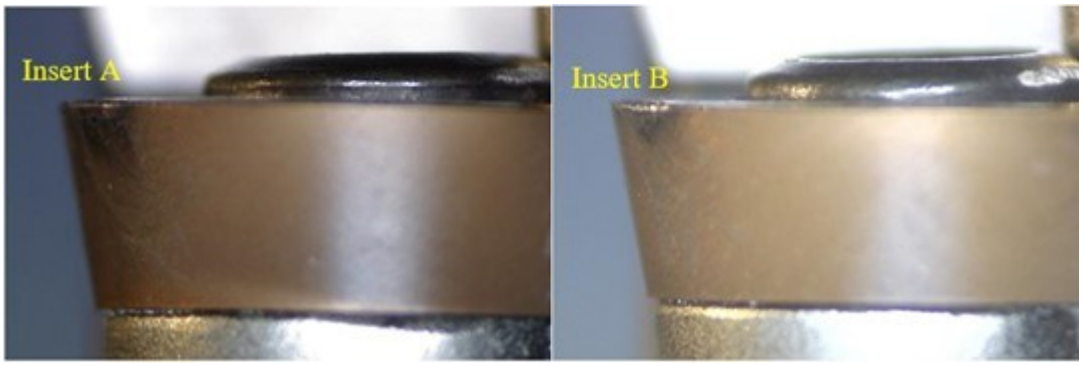

Figure 4.10 The wear images of insert A and B after milling three layers of the workpiece.

Table 4.5 The cutting radii and flank wear after milling three layers of the workpiece.

Measurement point	1	2	3	4	5
Tool radius (mm)	6.650	7.164	7.527	7.868	8.148
Radius wear (mm)	0.021	0.033	0.064	0.042	0.032
Measured V_B (mm)	0.032	0.061	0.120	0.095	0.092
Predicted V_B (mm)	0.029	0.0581	0.129	0.100	0.088
Error	10.34%	4.99%	6.98%	5.00%	4.55%

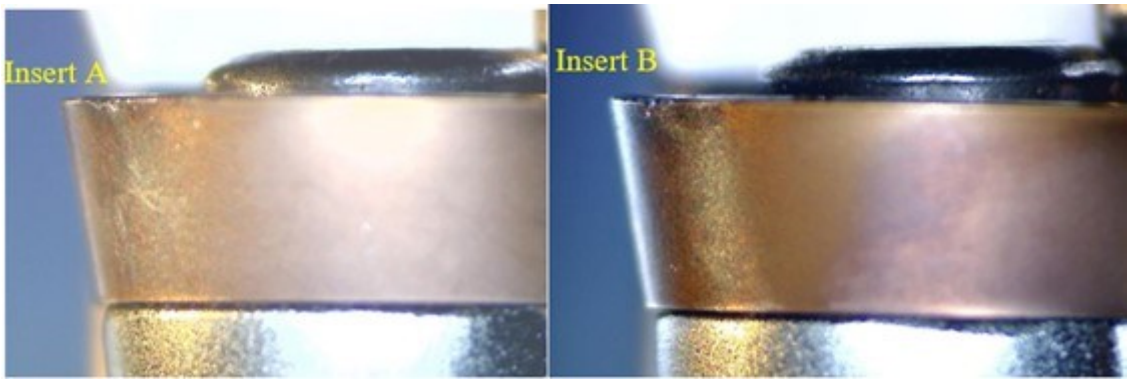

Figure 4.11 The wear images of insert A and B after milling four layers of the workpiece.

Table 4.6 The cutting radii and flank wear after milling four layers of the workpiece.

Measurement point	1	2	3	4	5
Tool radius (mm)	6.642	7.144	7.467	7.834	8.139
Radius wear (mm)	0.029	0.053	0.124	0.076	0.041
Measured V_B (mm)	0.037	0.091	0.221	0.171	0.094
Predicted V_B (mm)	0.035	0.083	0.238	0.160	0.093
Error	5.71%	9.64%	7.14%	6.88%	1.08%

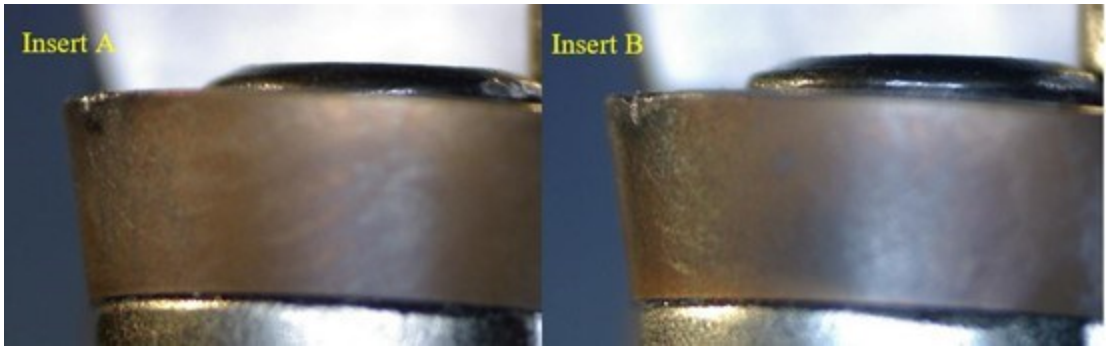

Figure 4.12 The wear images of insert A and B after milling five layers of the workpiece.

Table 4.7 The cutting radii and flank wear after milling five layers of the workpiece.

Measurement point	1	2	3	4	5
Tool radius (mm)	6.628	7.123	7.446	7.802	8.132
Radius wear (mm)	0.043	0.074	0.145	0.108	0.048
Measured V_B (mm)	0.048	0.110	0.271	0.211	0.101
Predicted V_B (mm)	0.052	0.117	0.282	0.233	0.109
Error	7.69%	5.98%	3.90%	9.44%	0.9%

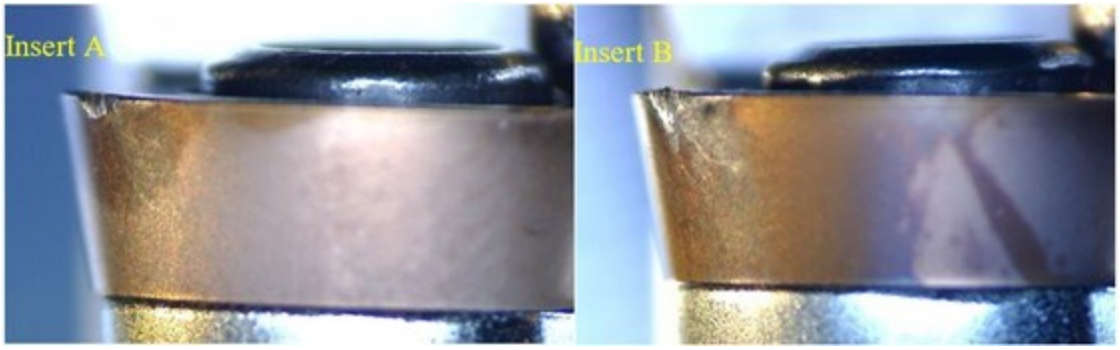

Figure 4.13 The wear images of insert A and B after milling six layers of the workpiece.

Table 4.8 The cutting radii and flank wear after milling six layers of the workpiece.

Measurement point	1	2	3	4	5
Tool radius (mm)	6.621	7.093	7.360	7.766	8.124
Radius wear (mm)	0.050	0.104	0.231	0.144	0.056
Measured V_B (mm)	0.070	0.186	chipping	chipping	0.134
Predicted V_B (mm)	0.064	0.173	0.495	0.336	0.145
Error	9.38%	7.51%	--	--	7.59%

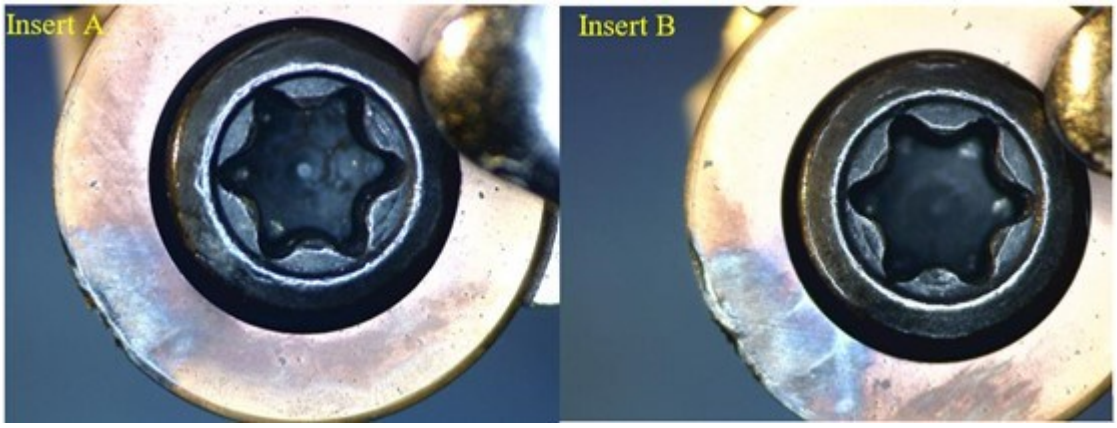

Figure 4.14 The inserts wear out after milling six layers of the workpiece.

It can be seen from the experimental results that after the first layer of milling, the tool inserts wear out with only small values, the maximum error between the predicted and measured flank wear land width is 7.69%, the maximum flank wear land width occurs at the measurement height 1 mm with a value of 0.080 mm. The tool is in the break-in wear period, and the tool flank wear is uniform. After milling two layers of the workpiece, the maximum flank wear land width still occurs at 1mm measurement height with the value of 0.081 mm, and the maximum predicted error is 8%, the tool flank wear is still uniform, and the cutting tool enters the steady-rate wear stage. After milling three layers of the workpiece, localized flank wear appears at 0.6 mm measurement location and the maximum flank wear land width increased to 0.12 mm, the maximum tool wear prediction error is 10.34%. The fourth and fifth layer further wears the inserts' flank face and the predicted flank wear land width errors are within 10 percent, it is ready to see the tool entering the failure stage. Chipping occurs on both inserts at measurement heights 0.6 mm and 0.8 mm after milling six layers of the workpiece, and the measured flank wear land width at these two locations beyond 0.3 mm, the tool is defective. The prediction errors at measurement

points without chipping are all less than 10 percent. The measured results verify the accuracy of the flank wear land width Equation 3.20.

From the results above, it can also be noticed that the tool insert radius wear increases faster at location P_3 and chipping at this location is the most obvious. As a result, P_3 is the critical tool wear location and measurement height 0.6 mm is the optimum measurement height when measuring this type of round insert milling tool for on-machine tool condition monitoring.

4.4 Application: the OMM tool wear threshold for roughing and finishing

In this section, a new approach has proposed to determine the threshold of round-insert face mill radius reduction for tool failure in roughing and finishing. The CNC controller needs the threshold to analyze the measured tool information and monitor the tool condition, providing timely alerts for tool replacement. In industry, except for the tool condition itself, the surface quality of the machined workpiece is also a necessary standard in finish machining. As a result, the surface roughness of the machined workpiece is the key to indicate tool life. In roughing, tool condition is the major concern, so the tool radius wear threshold can be determined by the flank wear land width using the flank wear equation.

The OMM tool wear threshold for finishing is to determine a maximum allowable tool radius wear by establishing the relationship between the tool cutting radius wear and the surface roughness of the workpiece for milling progress through experiments. The procedures for determining the OMM tool wear threshold are as follows:

- Collect the tool parameters, set the cutting parameters, and perform cutting operations
- During the machining, choose an appropriate interval for tool measurements and surface roughness measurements.
- Once the surface roughness of the workpiece increases beyond the desired value, record current tool wear types, find the critical tool wear location, collect the tool radius wear, and calculate the predicted tool flank wear land width.
- Compare the tool failure threshold regarding flank wear land width and machined workpiece surface roughness and determine an optimum tool radius wear threshold for roughing and finishing.

The OMM tool radius wear threshold is established based on each type of cutting tool and machining progress. In this section, the milling progress mentioned in the previous section is selected as a milling progress example to demonstrate the approach of determining the tool wear threshold in roughing and finishing. The EMR5R round insert mill is selected to remove a layer of the material of the 2Cr13 workpiece by 1 mm, the desired surface roughness of the machined workpiece in finishing surface roughness is set as 1.6 μm, and the surface roughness is measured by the TR280 surface roughness tester (see Figure 4.15). The surface roughness values are tested after the cutting tool removes one layer of the workpiece, Ra value of each measurement is the arithmetic mean of ten measure points on the workpiece surface, and the cutoff length and evaluation length are 0.8 mm and 4 mm respectively.

Figure 4.15 The surface roughness is measured after milling each 1mm layer of the workpiece.

The tool radii at measurement height 0.6 mm are selected as the optimum measurement height since the previous cutting results show that tool wears quicker at this location. The same experiment is conducted twice to ensure the universality of the results. The measurement results are shown in Table 4.9 and Table 4.10.

Table 4.9 The first tool and workpiece condition of each measurement.

Measurement no.	Tool radius wear at P_3	Predicted V_B at P_3	Workpiece Ra
1	0.020	0.036	1.052
2	0.031	0.056	1.256
3	0.059	0.109	1.493
4	0.131	0.252	1.587
5	0.140	0.271	1.637

Table 4.10 The second tool and workpiece condition of each measurement.

Measurement no.	Tool radius wear at P_3	Predicted V_B at P_3	Workpiece Ra
1	0.026	0.047	0.822
2	0.033	0.060	1.363
3	0.067	0.124	1.507
4	0.128	0.246	1.540
5	0.151	0.295	1.755

From the results of the two milling operations, it can be found that the surface roughness of the measured workpiece increases with the tool radius wear and flank wear. In the final cut, the measured workpiece surface roughness increases beyond the requirement surface roughness of 1.6 μm, thus the tool radius wear threshold in finishing should be the average of the tool radius wears (*DR*) after four cuts in the two cutting operations, that is 0.130 mm. It can also be noticed that in finishing, when the workpiece quality no longer meets the requirement, the flank wear land widths are still less than 0.3 mm.

As for the tool radius wear threshold in roughing, the tool flank wear at measurement height 0.6 mm can be calculated by the flank wear equation. According to the ISO-8688 standard, the tool flank wear should be no more than 0.3mm. In Equation 3.20, when h equals to 0.6 mm, and V_B is

0.3 mm, the tool radius wear *DR* can be calculated as 0.153 mm. So, the tool radius wear threshold for roughing is 0.153 mm at P_3.

Comparing the two tool radius wear thresholds based on the two standards, the threshold for finishing is smaller than the one for roughing, to satisfy the requirement of the workpiece, *DR* should be selected as 0.130 mm for the tool radius wear threshold in finishing.

After the OMM tool wear threshold is set, this approach is applied to a practical work. A new round-insert face mill is adopted, and it cuts a workpiece like before. The measurements are taken after milling every layer of the workpiece. The results are shown in Table 4.11.

Table 4.11 The verification of the OMM tool radius threshold.

Measurement no.	Tool radius wear at P_3 (mm)	Predicted V_B at P_3 (mm)	Measured Ra	Tool condition
1	0.021	0.038	0.945	Valid
2	0.040	0.073	1.126	Valid
3	0.079	0.148	1.256	Valid
4	0.112	0.213	1.479	Valid
5	0.132	0.255	1.687	Invalid
6	0.154	0.301	1.693	Invalid

In the fifth measurement, the tool wears increase beyond the OMM tool radius wear threshold, and the corresponding surface roughness of the workpiece is larger than the requirement *Ra*, while the tool flank wear land width is 0.255 mm, less than 0.3 mm. By observing the condition of the insert under the microscope, a build-up edge is found after the fifth cut, which further proves that the tool has become ineffective in finishing at this point (see Figure 4.16). During the sixth cut, the tool continues to cut the workpiece, the build-up edge detaches from the inserts and causes chipping, and the tool fails (see Figure 4.17). Thus, the concept of establishing the OMM tool radius threshold for roughing and finishing is feasible, and its reliability has been proved.

Figure 4.16 The build-up edge is found in the fifth measurement.

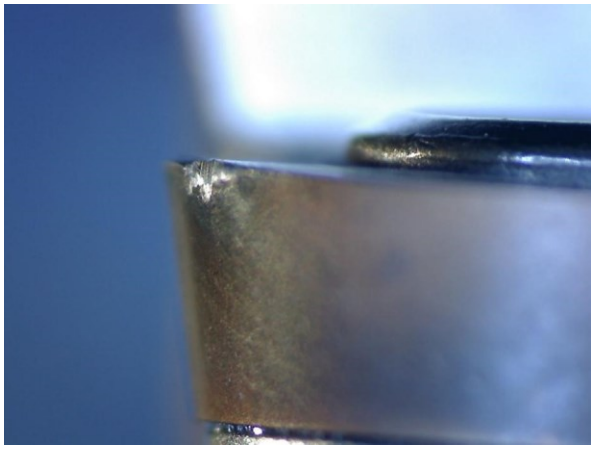

Figure 4.17 The chipping is found in the sixth measurement.

Chapter 5 Conclusion

This research proposed a novel and efficient method for tool condition using a laser tool setter to construct the on-machine measurement and on-machine tool condition monitoring system.

The model of a round insert indexable milling tool is established to demonstrate the geometry relationship between the tool flank wear land width and the tool cutting radius wear. Experiments are conducted to verify the reliability of this tool wear theory. A new approach has proposed to determine the tool radius threshold of round-insert face mill radius reduction for tool failure in roughing and finishing, and the reliability of the threshold has been proved.

With the tool flank wear mechanism and the OMM tool radius threshold being built, the CNC machine can automatically determine the tool wear condition during machining, and the relationship between the tool radius wear and workpiece surface roughness is established. The method of establishing the OMM tool radius wear threshold for roughing and finishing can be a reference and guidance for tool condition monitoring in practical industry machining.

Bibliography

[1] Cho M. W., Kim G.H., Seo T.I., Hong Y.C., and Cheng H.H., 2006, "Integrated machining error compensation method using OMM data and modified PNN algorithm." International Journal of Machine Tools and Manufacture, Vol. 46, No. 12-13, pp. 1417-1427.

[2] Vieira J.M., Baptista E.A., Araki L., Smith S., and Schmitz T., 2018, "The role of tool presetting in milling stability uncertainty." Procedia Manufacturing, Vol. 26, pp. 164-172.

[3] Chen Z., and Zhang J.L., 2013, "On-line tool wear measurement for ball-end milling cutter based on machine vision." Computers in industry, Vol. 64, No. 6, pp. 708-719.

[4] Test code for machine tools — Part 10: Determination of the measuring performance of probing systems of numerically controlled machine tools, 2022, ISO 230-10:2022.

[5] Fang Z., 2015, "Research and Application of the Cutter Geometry On-Machine Measurement Using Laser Tool Setters." Master Degree Thesis, Concordia University, Canada.

[6] Arnaud D., Lesko S., and Mozer W., 2004, "Cutting tool crater wear measurement with white light interferometry." Wear, Vol. 256, No. 1-2, pp. 56-65.

[7] Chang L., Ren C.Z., Wang G.F., Yang Y.W., and Zhang L., 2015, "Study on surface defects in milling Inconel 718 super alloy." Journal of Mechanical Science and Technology, Vol. 29, pp. 1723-1730.

[8] Tlusty J., and Masood Z., 1978, "Chipping and breakage of carbide tools." pp. 403-412.

[9] Ezugwu E.O., and Pashby I.R., 1992, "High speed milling of nickel-based superalloys." Journal of materials processing technology, Vol. 33, No. 4, pp. 429-437.

[10] Woo W.S., and Lee C.M., 2018, "A study on the edge chipping according to spindle speed and inclination angle of workpiece in laser-assisted milling of silicon nitride." Optics & Laser Technology, Vol. 99, pp. 351-362.

[11] Dirk B., Steiner M., and Krebs E., 2013, "Investigation of different hard coatings for micro-milling of austenitic stainless steel." Procedia Cirp, Vol. 7, pp. 246-251.

[12] Cedergren S., Olovsjö S., Sjöberg G., and Nyborg L., 2013, "The effects of grain size and feed rate on notch wear and burr formation in wrought Alloy 718." The International Journal of Advanced Manufacturing Technology, Vol. 67, pp. 1501-1507.

[13] Chao X., Wang D., and Zhang J.J., 2022, "Wear Mechanisms and Notch Formation of Whisker-Reinforced Alumina and Sialon Ceramic Tools during High-Speed Turning of Inconel 718." Materials, Vol. 15, No. 11, pp. 3860.

[14] Chandrasekaran H., and Johansson J.O., 1994, "Chip flow and notch wear mechanisms during the machining of high austenitic stainless steels." CIRP annals, Vol. 43, No. 1, pp. 101-105.

[15] Su Y., He N., Li L., and Li X.L., 2006, "An experimental investigation of effects of cooling/lubrication conditions on tool wear in high-speed end milling of Ti-6Al-4V." Wear, Vol. 261, No. 7-8, pp. 760-766.

[16] Luo X., Cheng K., Holt R., and Liu X.P., 2005, "Modeling flank wear of carbide tool insert in metal cutting." Wear, Vol. 259, No. 7-12, pp. 1235-1240.

[17] Jozić S., Branimir L., and Dražen B., 2014, "A new mathematical model for flank wear prediction using functional data analysis methodology." Advances in Materials Science and Engineering.

[18] Su J.C., Huang C.K., and Tarng Y.S., 2006, "An automated flank wear measurement of microdrills using machine vision." Journal of Materials Processing Technology, Vol. 180, No. 1-3, pp. 328-335.

[19] Kasim M.S., Haron C.C., Ghani J.A., Sulaiman M.A., and Yazid M.Z.A., 2013, "Wear mechanism and notch wear location prediction model in ball nose end milling of Inconel 718." Wear, Vol. 302, No. 1-2, pp. 1171-1179.

[20] Bermingham M.J., Sim W.M., Kent D., Gardiner S., and Dargusch M.S., 2015, "Tool life and wear mechanisms in laser assisted milling Ti–6Al–4V." Wear, Vol. 322, pp. 151-163.

[21] Odedeyi P.B., Abou-El-Hossein K., and Liman M., 2017, "An experimental study of flank wear in the end milling of AISI 316 stainless steel with coated carbide inserts." In Journal of Physics: Conference Series, Vol. 843, No. 1, 012058.

[22] Bermingham M.J., Sim W.M., Kent D., Gardiner S., and Dargusch M.S., 2015, "Tool life and wear mechanisms in laser assisted milling Ti–6Al–4V." Wear, Vol. 322, pp. 151-163.

[23] Emre A., Gokkaya H., Karatas M.A., and Ozkan D., 2020, "Analysis of surface roughness and flank wear using the taguchi method in milling of NiTi shape memory alloy with uncoated tools." Coatings, Vol. 10, No. 12, pp. 1259.

[24] International Organization for Standardization (ISO) 1989 Tool life testing in milling, ISO 8688-1 (Switzerland: International Organization for Standardization)

[25] International Organization for Standardization (ISO) 1989 Tool life testing in milling, ISO8688-2 (Switzerland: International Organization for Standardization)

[26] Cook N.H., 1973, “Tool Wear and Tool Life.” Journal of Engineering for Industry, Vol. 95, pp. 931-938.

[27] Alauddin M., El Baradie M.A., and Hashmi M.S.J., 1997, "Prediction of tool life in end milling by response surface methodology." Journal of Materials Processing Technology, Vol. 71, No. 3, pp. 456-465.

[28] Khorasani A.M., Mohammad R., Soleymani Y., and Safizadeh M.S., 2011, "Tool Life Prediction in Face Milling Machining of 7075 Al by Using Artificial Neural Networks (ANN) and Taguchi Design of Experiment (DOE)." International Journal of Engineering and Technology, Vol. 3, No. 1, pp. 30.

[29] Karandikar J.M., Abbas A.E., and Schmitz T.L., 2014, "Tool life prediction using Bayesian updating. Part 1: Milling tool life model using a discrete grid method." Precision Engineering, Vol. 38, No. 1, pp. 9-17.

[30] Cyril D., Karandikar J., Nath C., Journeaux A.C., El Mansori M., and Kurfess T., 2016, "Tool life predictions in milling using spindle power with the neural network technique." Journal of Manufacturing Processes, Vol. 22, pp. 161-168.

[31] Yang Y.F., Guo Y.L., Huang Z.P., Chen N., Li L., Jiang Y.F., and He N., 2019, "Research on the milling tool wear and life prediction by establishing an integrated predictive model." Measurement, Vol. 145, pp. 178-189.

[32] Wang C.D., Ming W.W., and Chen M., 2016, "Milling tool's flank wear prediction by temperature dependent wear mechanism determination when machining Inconel 182 overlays." Tribology International, Vol. 104, pp. 140-156.

[33] Palanisamy P., Rajendran I., and Shanmugasundaram S., 2008, "Prediction of tool wear using regression and ANN models in end-milling operation." The International Journal of Advanced Manufacturing Technology, Vol. 37, pp. 29-41.

[34] Banda T., Liu Y.C., Farid A.A., and Lim C.S., 2023, "A machine learning model for flank wear prediction in face milling of Inconel 718." The International Journal of Advanced Manufacturing Technology, Vol. 126, No. 3-4, pp. 935-945.

[35] Gouarir A., Martínez-Arellano G., Terrazas G., Benardos P., and Ratchev S.J.P.C., 2018, "In-process tool wear prediction system based on machine learning techniques and force analysis." Procedia CIRP, Vol. 77, pp. 501-504.

[36] Uros Z., Cus F., and Kiker E., 2009, "Adaptive network based inference system for estimation of flank wear in end-milling." Journal of Materials Processing Technology, Vol. 209, No. 3, pp. 1504-1511.

[37] Kıvak T., 2014, "Optimization of surface roughness and flank wear using the Taguchi method in milling of Hadfield steel with PVD and CVD coated inserts." Measurement, Vol. 50, pp. 19-28.

[38] Rodriguez C.E.P., and Gilberto F.M., 2010, "Reliability concepts applied to cutting tool change time." Reliability Engineering & System Safety, Vol. 95, No. 8, pp. 866-873.